SRC, DIS, and the EMC effect

A LOI submitted to the JLab PAC 35, Jan 2010

O.Chen, E. Piasetzky, I. Korover, J. Lichtenstadt, I. Pomerantz,
and R. Shneor (contact person)
Tel Aviv University, Tel Aviv, Israel

R. Guy
Lawrence Berkeley National Lab, Berkeley, CA, USA.

W. Bertozzi, S. Gilad, and V. Sulkosky (spokesperson)
Massachusetts Institute of Technology, Cambridge, MA, USA

B.D. Anderson, A.R. Baldwin, G. Petratos,
and J.W. Watson (spokesperson),
Kent State University, Kent, OH, USA

J.P. Chen, J.-O. Hansen, D.W. Higinbotham (spokesperson), M. Jones,
J.J. LeRose, D. Meekins, A. Saha, and S. A. Wood
Thomas Jefferson National Accelerator Facility, Newport News, VA, USA

W. Boeglin and P. Markowitz
Florida International University, Miami, FL, USA

A. Beck and S. Maytal-Beck
Nuclear Research Center Negev, Beer-Sheva, Israel

L. Weinstein
Old Dominion University, Norfolk, VA, USA

M. Sargsian
Florida International University, Miami, FL, USA

I. Cloet, and G. A. Miller
University of Washington, Seattle, WA, USA

C. Ciofi degli Atti, L.P. Kaptari, V. Palli, and C.B. Mezzetti
University of Perugia, Perugia, Italy

M. Strikman, and M. Alvioli
Pennsylvania state University

L. Frankfurt
Tel Aviv University, Tel Aviv, Israel

I. Introduction

I.1 The EMC effect

Nucleon properties are modified in the nuclear medium. It is a major challenge of modern nuclear physics to identify and study these non trivial, small but important modifications of a single nucleon due to its presence in the nuclear medium.

The best known example of such a change between a bound and free nucleon is the so called EMC effect which was discovered in the mid 80s [1] and since confirmed many times [2-7]. The EMC effect is the reduction of the cross section for scattering off a nucleon bound in a nucleus relative to that of a free nucleon. A comprehensive review of the EMC effect can be found in [8, 9] and the references therein.

While the EMC and other modifications have been observed, a precise explanation of their origin currently eludes theoretical understanding. In general, two classes of explanations have been proposed. The first involves effects stemming from nuclear structure. A second class of explanations put forward is one in which the internal structure of the nucleon is modified by the external influence of the nuclear medium on the nucleon wave function.

Recent published result of the EMC effect measured on light nuclei at JLab [7] shows that the EMC is not a function of the atomic mass A or the average nuclear density, as was previously assumed by some models/calculations. As the authors claim;" The data … suggest that the nuclear dependence of the quark distributions may depend on the local nuclear environment".

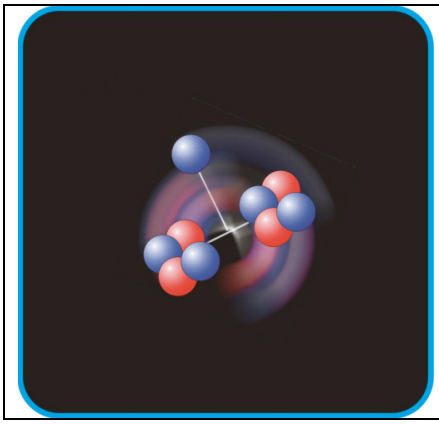

Fig 1: The most telling example is beryllium. The beryllium nucleus contains two clusters that resemble helium nuclei. This structure may explain new data [7] showing that helium and beryllium have a similar EMC effect despite their different masses and average densities.

We propose to study the EMC effect with the better resolving power allowed by semi-inclusive measurements in order to identify which nucleons in the nucleus contribute to the effect and what the relevant local densities are.

I.2 Short Range Correlation (SRC) in nuclei

We consider SRC nucleon pairs in nuclei, in which the separation distance between nucleon centers is approximately one femtometer (fm) or smaller. In momentum space, a SRC pair is characterized by a large relative momentum and a small center-of-mass (cm) momentum, where large and small are relative to k_F , the Fermi momentum [10-12].

In the last decade, high energy large momentum transfer studies of SRC at JLab [13-18] and BNL [19-22] support a 'standard' theoretical picture of the short distance structure of nuclei:

●The probability for a nucleon to have momentum above the Fermi sea level in medium nuclei is ~25%.

●Almost all nucleons above the Fermi-Sea are part of 2N-SRC (74-92 %).

● These SRC pairs move inside the nucleus with c.m. motion of σ~140 MeV/c.

● The 2N-SRC consists of: **n-p pairs (90%), p-p pairs(5%), n-n pairs(5%).**

● The dominant NN force in the 2N-SRC is the tensor force.

A pie chart that represents our 'standard' picture of ^{12}C short range structure is shown in Fig 2.

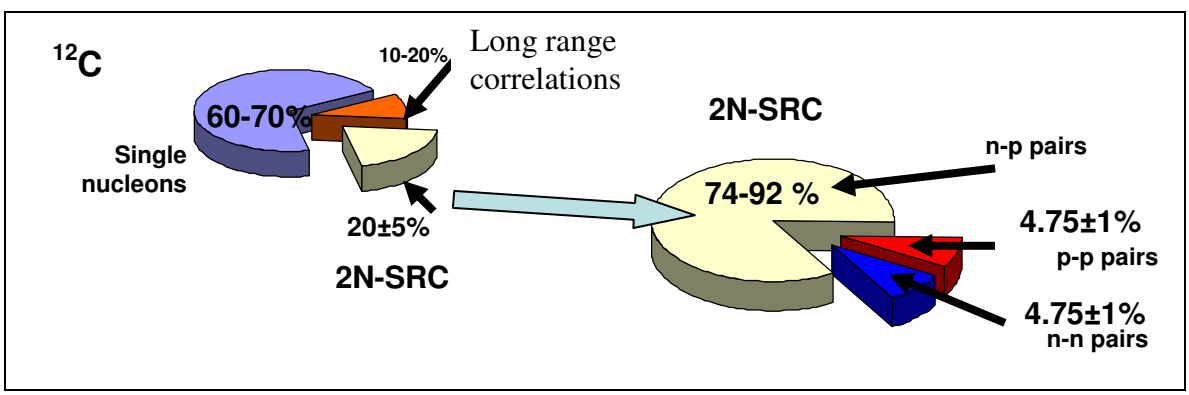

Fig2: The short distance structure of ^{12}C as deduced from recent measurements.

We propose to determine the SRC contribution to the EMC effect by comparing the EMC effect from nucleons in a SRC (~20% of nucleons in the nucleus) to the EMC effect from mean-field nucleons (~80 of the nucleons).

I.3 SRC and the EMC effect

Assuming that the EMC effect is due to a difference in the quark's distribution in bound and free nuclei, two approaches exist that lead to very different answers as to how the EMC strength is distributed between the SRC and the mean field nucleons in nuclei.

One hypothesis is that can be the cause of the EMC is the fact that the quarks are in the mean field of the nucleus. Fig 3 shows a schematic representation of a typical NN potential as a function of the distance between the nucleon's centers. What is shown in the figure is the dominant scalar potential that creates the maximum attraction at distances typical to those between the mean field nucleons in nuclei. A reasonable assumption would be that at the distance where the mean field attraction is maximal, the change in the quarks structure function due to this field is also maximal.

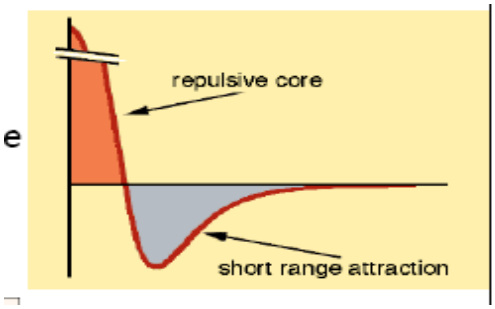

Fig 3: A schematic presentation of the dominant scaler NN potential as a function of the distance between the nucleons.

A different approach to answer the same question can be to claim that the EMC effect is mainly from nucleons in SRC pairs. These nucleons have large momentum, large virtuality and a local environment that differs more from free space than that of the other nucleons in the nucleus. Therefore, it might not be a surprise to find that they exhibit the largest changes in their internal structure. A recent measurement at JLab (E03-104), not yet published, seems to indicate that the medium modifications become larger with an increase of the nucleon virtuality [24], see Figure 4. In the proposed SRC experiment the virtuality is much larger than in this experiment which scattered off mean field nucleons in ^{4}He.

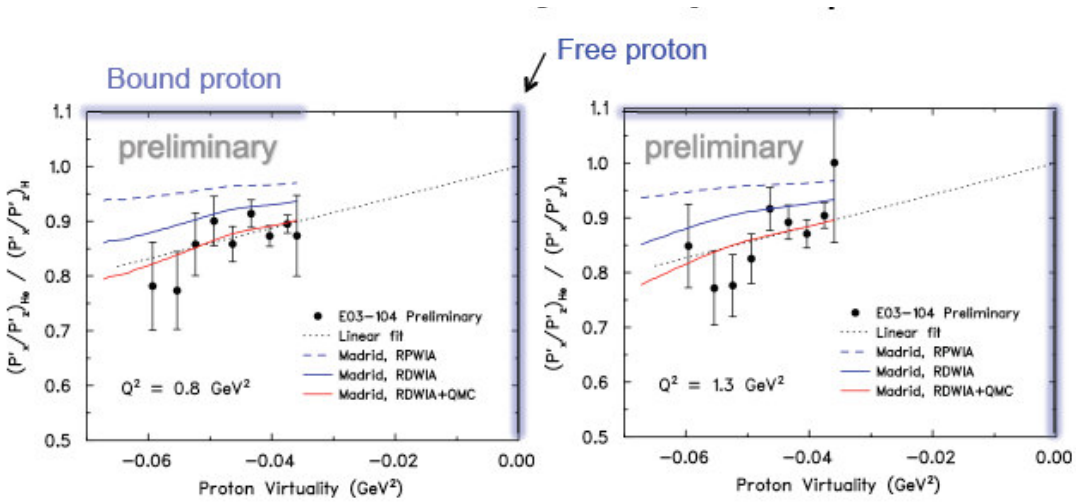

Fig 4: Preliminary results from E03-104 showing deviation from the free nucleon as a function of the virtuality. The latter is defined as the difference between the reconstructed 4- momentum square of the quasi elastic proton and its free mass square.

Note that the difference between these two approaches, which we propose to check by measurement, has far reaching consequences from the structure of the deuteron to neutron-stars.

The original EMC measurement, more than 20 years ago, used the deuteron as a free proton and neutron system and measured the ratio of inclusive DIS on nuclei to deuterium. This is a good approximation since the deuteron is loosely bound (~2 MeV), the distance between the nucleons is large (~2 fm), and the EMC effect is negligible. But what will happen if we do the DIS scattering off a nucleon with large momentum at the tail of the deuteron wave function? Would the EMC there be larger or smaller than in a heavy nucleus?

It is clear that reducing the nuclear density will reduce the EMC effect, but what happens in denser nuclear systems like neutron-stars? Is the EMC larger or smaller than in nuclei?

We propose to address these questions by studying the EMC effect on nucleons which are partners in SRC pairs. In models that assume the EMC effect to depend on the virtuality of the interacting nucleon, defined via the kinematics of the spectator, we can expect the EMC effect to be substantially enhanced compared to the effect measured in the inclusive measurements.

I.4 Study of SRC in the DIS domain by semi-inclusive measurement

In the QE region, a high-momentum point-interacting probe knocks a proton out of a nucleus, leaving the residual nucleus nearly unaffected. If, on the other hand, the proton being struck is a part of an SRC pair, the high relative momentum in the pair would cause the correlated nucleon to recoil and be ejected with high-momentum, almost equal in size and opposite in direction to that of the initial momentum of the struck nucleon (see Fig. 5).

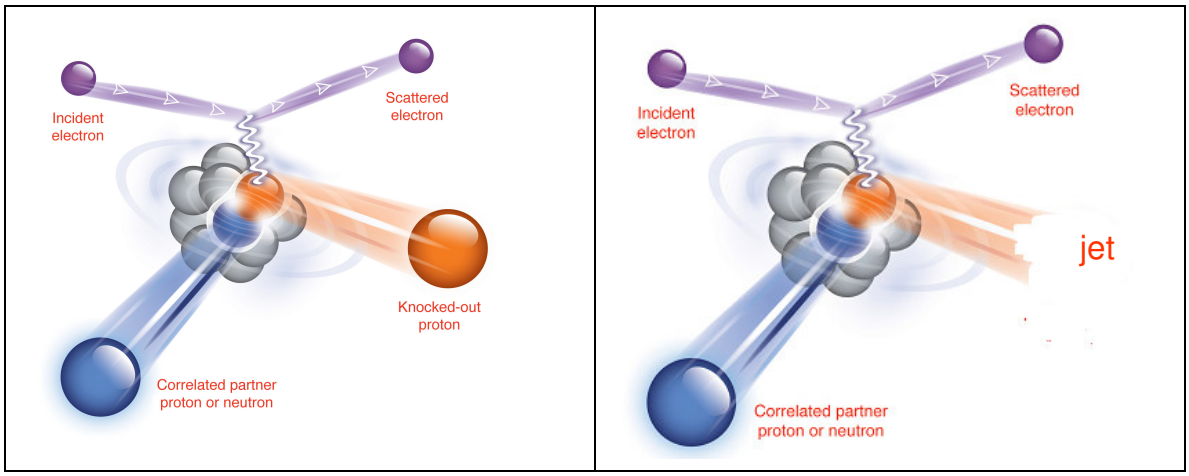

Fig 5: QE (left) and DIS (right) electron scattering off a nucleon in nuclei.

In DIS kinematics (W > 2 GeV) the virtual photon interacts with a quark in the nucleon, destroying the nucleon and creating a jet of particles in the momentum transfer direction (marked as 'jet' in Fig 5). If the standard picture described above for SRC is correct one can expect that if the proton being struck is part of a SRC pair, the high relative momentum in the pair would cause the correlated nucleon to recoil and be ejected with high-momentum almost equal in size and opposite in direction to that of the struck proton as in the QE domain.

An approved 12 GeV proposal [23] will study scaling in the DIS, using inclusive (e,e') scattering, the same way that it was done in the QE domain with CLAS/Hall B [13,14]. We propose here to do a semi-inclusive measurement and to detect the recoil high momentum nucleon in coincidence with the DIS off its correlated partner.

Based on the theoretical understanding of SRC in nuclei as discussed above we propose to tag the DIS events with high momentum recoil nucleons in the direction which is defined by the kinematics of the DIS.

We propose to measure DIS events off a deuteron target but with constrained kinematics which correspond to scattering off a nucleon in the deuteron with high momentum (300-600 MeV/c). Scattering off one nucleon in coincidence with the other nucleon recoiling with high momentum is a signature of SRC.

Figure 6 shows the cross section for the (e,e'p_back) semi-inclusive scattering off the deuteron calculated as described in ref [27]. As demonstrated in the figure, the backward yield of high momentum protons is dominated by the SRC and the FSI are only a small correction.

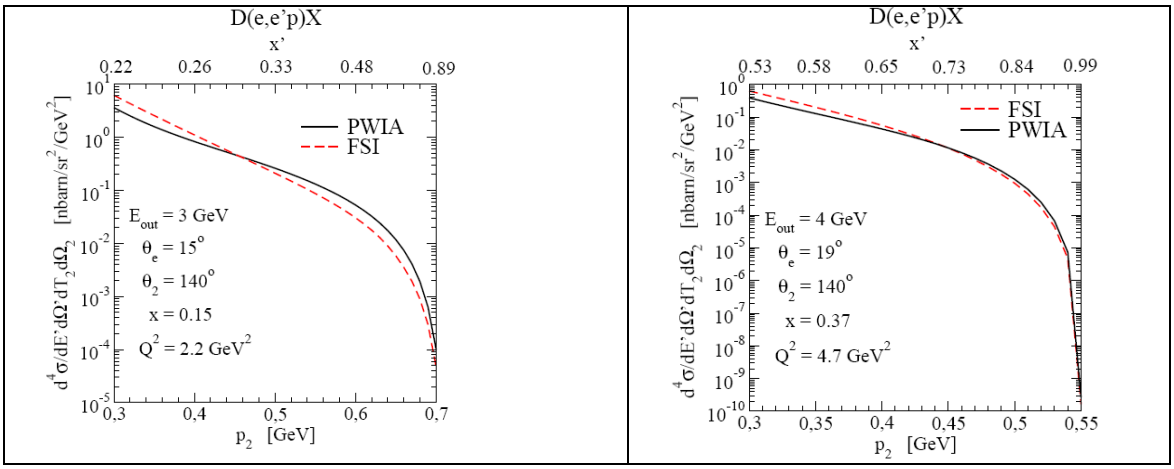

Fig 6: The predicted semi- inclusive cross section for the deuteron with a backward scattered high momentum proton [27].

The same calculations done assuming an EMC effect as predicted by the suppression of the PLC model [30] and no EMC effect are shown for the x'=0.6 (see the definition of x' in the following sector) kinematics in Figure 7.

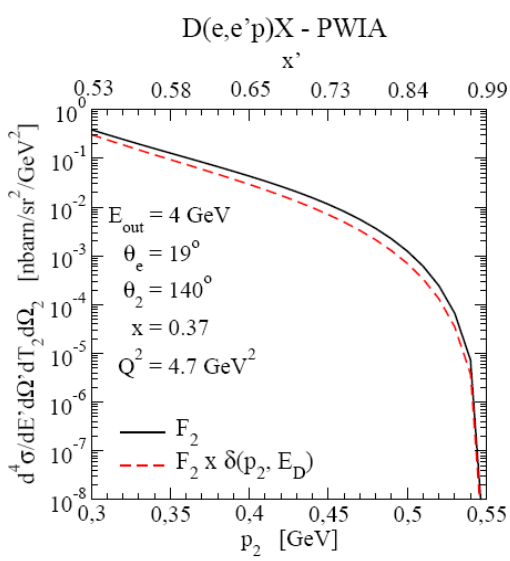

Fig 7: The predicted semi- inclusive cross section for deuteron with a backward scattered high momentum proton with and without EMC effect as predicated by [30].

In a light nucleus, heavier than deuteron, the tagging by high momentum recoil nucleon should favor a DIS electron scattering off a nucleon in a 2N-SRC and therefore will enhance the EMC effect. We also propose to do the measurements on ^{4}He, which is the lightest nucleus (minimal FSI) that have a large EMC effect [7].

I.5 The Formalism for inclusive and semi-inclusive DIS

The inclusive cross section for an electron scattering off a free nucleon at rest in the laboratory frame can be expressed in the DIS region in terms of the structure functions F_1 and F_2:

$$\frac{d^3\sigma}{d\Omega dE'} = \left(\frac{d\sigma}{d\Omega}\right)_{Mott} \cdot \left[\frac{1}{\omega} F_2(x_B, Q^2) + \frac{2}{M} F_1(x_B, Q^2) \cdot \tan^2(\theta/2)\right],$$

where the Mott cross section is the cross section to scatter off a point charge, θ is the electron scattering angle in the Lab frame, Q^2 is the four momentum transfer, x_B is the Bjorken scaling factor given by:

$$x_B = \frac{Q^2}{2M\omega}.$$

The structure functions F_1 and F_2 are related by R, the ratio between the cross sections for longitudinal and transverse scattering. Assuming that for the free nucleon R is known, the measurement of inclusive scattering off a nucleon allows extracting the structure function F_2:

$$F_2(x, Q^2) = \left[\frac{d^2\sigma/d\Omega dE'}{(d\sigma/d\Omega)_{Mott}}\right] \cdot \left[\frac{\omega\varepsilon(1 + R(x, Q^2)}{1 + \varepsilon R(X, Q^2)}\right],$$

where ε is….

An important kinematical parameter that defines the DIS region is the total hadronic mass squared which is given for a free nucleon at rest as:

$$W^2 = M^2 - Q^2 + 2 \cdot M \cdot \omega$$

When scattering off a nucleon in nuclei, the movement of the nucleon needs to be taken into account. For a free nucleon moving in the Lab frame, the scaling parameter is

$$x' = \frac{Q^2}{2p \cdot q},$$

where p and q are the four vectors of the nucleon and the photon respectively.

Notice that for a nucleon at rest:

$p = (M, \vec{0})$ and $x' = x_B$.

In a deuteron, one can express x' in terms of the measured recoil tagging nucleon:

$$x' = \frac{Q^2}{2 \cdot [(m_d - E_2) \cdot \nu + p_{2.} \cdot q \cdot \cos(p_2.q)]},$$

where E_2 and p_2 are the energy and momentum of the recoil nucleon.

For a free nucleon moving with momentum p in the Lab frame the total hadronic mass squared is:

$$W'^2 = M^2 - Q^2 + 2 \cdot p \cdot q = M^2 - Q^2 + 2E_p \cdot \omega - 2\vec{p} \cdot \vec{q}$$

For a deuteron or correlated pair with no cm motion in the laboratory this can be expressed in terms of the recoil spectator momentum:

$$W'^2 = M^2 - Q^2 + 2E_p \cdot \omega + 2\vec{p}_s \cdot \vec{q} = M^2 - Q^2 + 2E_p \cdot \omega + 2\sqrt{Q^2 + \omega^2} \cdot p_s \cdot \cos(\theta)$$

Where θ is the angle between the photon and the recoil nucleon direction and $q = \sqrt{Q^2 + \omega^2}$.

To ensure a DIS process, we require for the moving nucleon:

$$W'^2 \geq 4GeV^2.$$

For a deuteron, even in the presence of FSI, the cross section for the semi-inclusive process is given in [25-27] by:

$$\frac{d^4\sigma}{dxdQ^2 d\vec{p}_2} = K \cdot n_D(\vec{p}_2, \vec{q}) \cdot \frac{x}{x'} \cdot F_2^*(x'),$$

where F* is the medium modified structure function of the nucleon in the deuteron, K is a kinematics factor given in [27] and n_D is the distorted momentum distribution of the deuteron [see eq. 14 in Ref. 27].

A bound nucleon at rest is also off its energy shell. To match more accurately off-shell and on shell kinematics at intermediate Q^2 one can parameterize F_2^* as a function of the invariant mass of the system produced in the virtual photon - bound nucleon scattering and Q^2.

II. Details of the proposed measurements

II.1 The proposed kinematics

We propose to measure the semi-inclusive cross section with the scattered electron detected simultaneously at two kinematics: one corresponds to x'=0.2-0.3 where no EMC effect is expected and the other at x'=0.6-0.7 where the EMC effect is expected to be maximal. The scattered electrons will be detected in coincidence with recoil protons with momentum of 300-600 MeV/c that will emerge over a large fraction of the backward hemisphere.

II.2 Experimental setup

We propose to do the measurement in Hall A using the two high resolution spectrometers (HRSs) in coincidence with a dedicated large angle proton detector LAD (see appendix I). The incident beam is 10.9 GeV and the two HRSs are set at 3 GeV / 15^0 and 4 GeV / 19^0 on both sides of the beam, to measure the electrons at the x'~0.3 and x'~0.6 kinematics simultaneously. The kinematic settings for these two measurements are :

HRS _right:

E_{in} = 10.9 GeV
E' = 3 GeV
$\theta_{e'} = 15^0$

Q^2 = 2.2 GeV^2
q = 8 GeV/c
$\theta_q = -5.5^0$
$x_B = 0.15$

For 400 MeV/c recoil proton:

Angle with respect to q [deg]	x'
100	0.179
120	0.216
140	0.259
160	0.297

HRS_left:
E_{in} = 10.9 GeV
E' = 4 GeV
$\theta_{e'} = 19^0$

Q^2 = 4.75 GeV^2
q = 7.2 GeV/c
$\theta_q = -10.4^0$
$x_B = 0.37$

For 400 MeV/c recoil proton:

Angle with respect to q [deg]	x'
100	0.439
120	0.532
140	0.643
160	0.744

For the proton detection, we propose to use the LAD detector. For this measurement, we plan to maximize the coverage of the backward hemisphere on both sides of the beam line at a distance of about 4 meters from the target. More details about the LAD detector can be found in Appendix I.

II.3 Rates

See appendix II

The tables below show the number of semi-inclusive events expected in 300 Hr of beam. The statistical uncertainties are also shown.

Table1: The number of semi-inclusive events as a function of the recoil angle [deg] and momentum [MeV/c], for x = 0.15. The expected statistical uncertainties are shown in parentheses.

$\theta_2 \setminus p_2$	*300*	*400*	*500*	*Total*
90	95300 (0.3%)	24600 (0.7%)	18600 (0.8%)	138500 (0.3%)
100	85100 (0.4%)	29700 (0.6%)	15400 (0.9%)	130200 (0.3%)
110	73200 (0.4%)	24500 (0.7%)	12000 (1%)	109700 (0.3%)
120	60600 (0.4%)	19300 (0.8%)	8800 (1.2%)	88700 (0.4%)
130	47900 (0.5%)	14500 (0.9%)	6000 (1.6%)	68400 (0.4%)
140	35800 (0.6%)	10200 (1.1%)	3700 (2.1%)	49700 (0.5%)
150	24600 (0.7%)	6600 (1.4%)	2100 (2.9%)	33300 (0.6%)
160	14300 (0.9%)	3600 (2.0%)	1000 (4.5%)	18900 (0.8%)
Total	436800 (0.2%)	133000 (0.3%)	67600 (0.4%)	637400 (0.1%)

Table 2: Same as the above for x=0.37.

$\theta_2 \setminus p_2$	*300*	*400*	*500*	*Total*
90	23400 (0.7%)	8100 (1.2%)	4100 (1.8%)	35600 (0.6%)
100	19400 (0.8%)	6100 (1.4%)	2700 (2.3%)	28200 (0.7%)
110	15200 (0.9%)	4300 (1.8%)	1600 (3.2%)	21100 (0.8%)
120	11200 (1.1%)	2700 (2.4%)	600 (6.5%)	14500 (1.0%)
130	7800 (1.3%)	1400 (3.6%)	200 (15%)	9400 (1.2%)
140	5100 1.6%)	700 (5.8%)	N/A	5800 (1.7%)
150	3000 (2.2%)	200 (15%)	N/A	3200 (2.4%)
160	1500 (3.3%)	N/A	N/A	1500 (3.3%)
Total	86600 (0.4%)	23500 (0.8%)	9200 (1.4%)	119300 (0.3%)

For momentum bins of 300±50, 400±50, 500±50 and angular bins of 10^0 from 90^0 to 160^0 the expected statistical error is typically better than 1-2% per bin. The systematic error in the ratio of the two kinematics is also small (~1%)due to the common beam, common target, and almost identical spectrometers. We therefore expect the uncertainty in the ratio of the measured in-medium structure functions that reflects the EMC to be dominated by the theoretical uncertainties. The later will be tested by the data itself.

II.4 Measurement plan and Beam time request

We estimate about 100 Hr for setup and calibration, 300 Hr of data taking with deuteron and 200 Hr with ^{4}He. Total of 600 Hr (25 days). The exact run plan will be part of the full proposal.

II.4 The road to a full proposal

Following endorsement by the PAC, we plan to make a more detailed design of the LAD spectrometer, taking into account the constrains in the area. This will allow detailed simulation of the expected rates, better estimate of the uncertainties, and a submission of a more detailed ran plan for the PAC approval.

Appendix I: The LAD configuration and performances

I.1 Introduction

To perform the above measurements, we propose to incorporate a "backward" Large Acceptance Detector (LAD) into the 12 GeV experimental Hall A setup. This detector will measure the recoil protons in coincidence with scattered electrons detected in one of the HRSs.

To achieve the goal with a low cost, we propose to use the TOF counters of the current CLAS that will not be used as part of CLAS12.

Figure I.1 shows the CLAS detector with the TOF counters. We propose to use the two backward panels of each sector with a total of 6 panels and 23 counters per panel. The counters are 3.5-4.5 meters long with a PMT on each end. The performances of these counters are well known and documented [32].

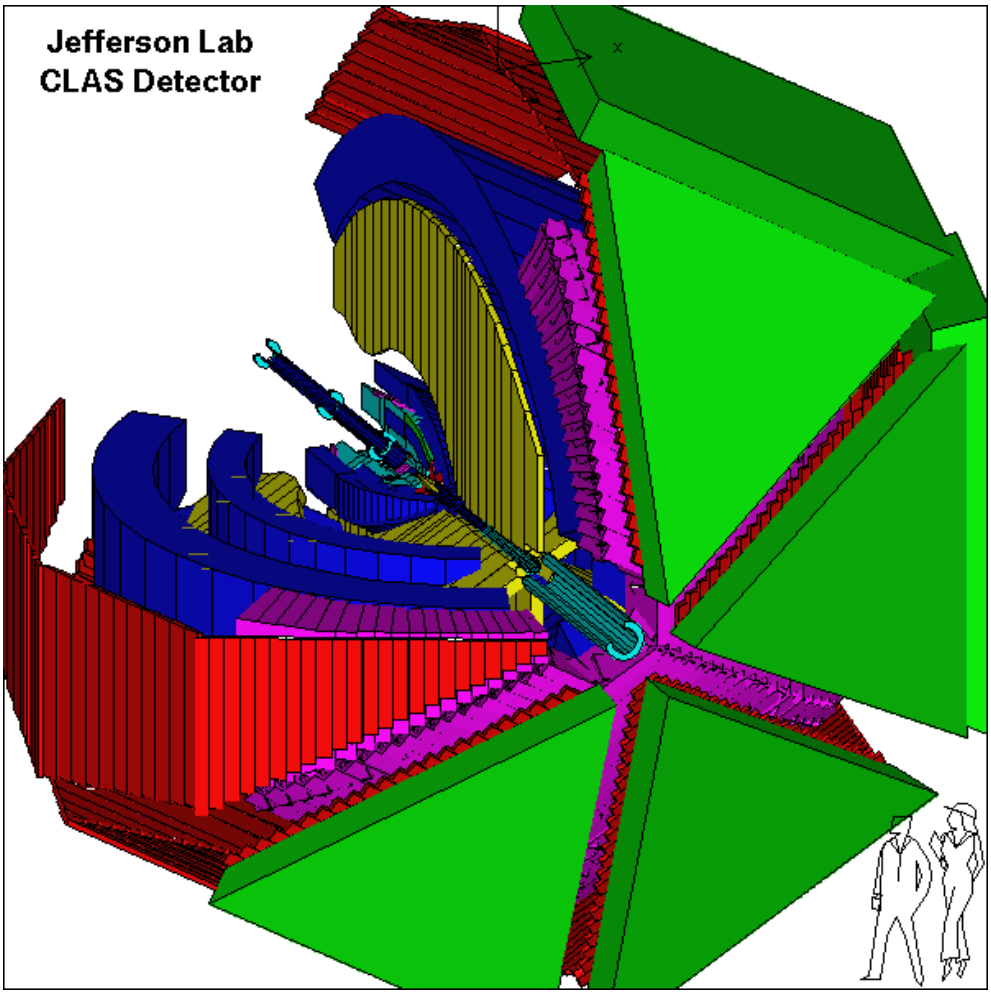

Figure I.1: The CLAS detector. The TOF panels to be used for LAD are shown in red.

Based on available data from Hall B and simulation, here we discuss some of the expected performance of the proposed LAD. The characteristics of the TOF scintillators are given in Table 1.

Table 1: Dimensions of the large-angle TOF scintillators. All counters are 5.08 cm thick.

Scintillator number	Width (cm)	Length (cm)	Light guide configuration	PMT	Nominal lab angle (deg)	Nominal distance from target (cm)
40a	22	416.3	Bent	XP4312B/D1	89.3	414
40b	22	410.5	Bent	XP4312B/D1	92.2	409
41a	22	404.8	Bent	XP4312B/D1	95.3	405
41b	22	399.0	Bent	XP4312B/D1	98.4	402
42a	22	393.3	Bent	XP4312B/D1	101.6	400
42b	22	387.5	Bent	XP4312B/D1	104.8	399
43a	22	380.1	Bent	XP4312B/D1	108.8	402
43b	22	363.5	Bent	XP4312B/D1	112.0	395
44a	22	347.0	Bent	XP4312B/D1	114.9	389
44b	22	330.4	Bent	XP4312B/D1	118.1	384
45a	22	313.9	Bent	XP4312B/D1	121.4	381
45b	22	297.3	Bent	XP4312B/D1	124.7	378
46a	22	280.8	Bent	XP4312B/D1	128.0	377
46b	22	264.2	Bent	XP4312B/D1	131.4	378
47a	15	246.8	Straight	XP2262	134.2	379
47b	15	235.4	Straight	XP2262	136.5	380
48a	15	224.0	Straight	XP2262	138.8	383
48b	15	212.7	Straight	XP2262	141.0	385
35	22	445.1	Bent	XP4312B/D1	75.7	457
36	22	439.3	Bent	XP4312B/D1	78.2	446
37	22	433.6	Bent	XP4312B/D1	80.8	437
38	22	427.8	Bent	XP4312B/D1	83.5	428
39	22	422.0	Bent	XP4312B/D1	86.3	421

I.2 Angular coverage

In general, the LAD will be designed to be flexible and to fit both Hall A and Hall C for configurations that fit the need of each particular experiment. For this measurement, we propose to set the sectors to cover the largest possible fraction of the backward hemisphere. For the rate calculation we assume coverage of 50% of the full backward hemisphere. A detailed GEANT simulation of the setup will be presented with the full proposal.

.

I.3 Particle identification

In Fig. I.2 the energy loss in the first layer of the CLAS scintillators is shown versus the velocity of the particle determined from the TOF. The energy loss is corrected for the light attenuation for each individual PMT. The position determination along the scintillator bars is determined using the time difference measured by the two PMTs on each scintillator. This is a standard CLAS procedure. The line shows the cut used to identify proton with $\beta < 0.9$.

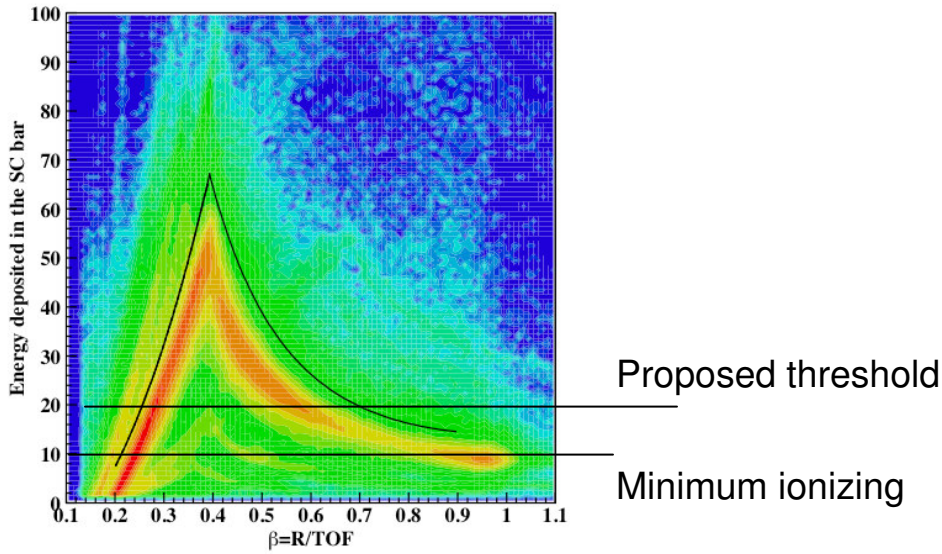

Figure I.2: The energy loss in the CLAS scintillators versus the β as determined from the TOF.

The energy loss per cm in the plastic and the TOF per meter of flight path are shown in figure I.3 from Geant simulations.

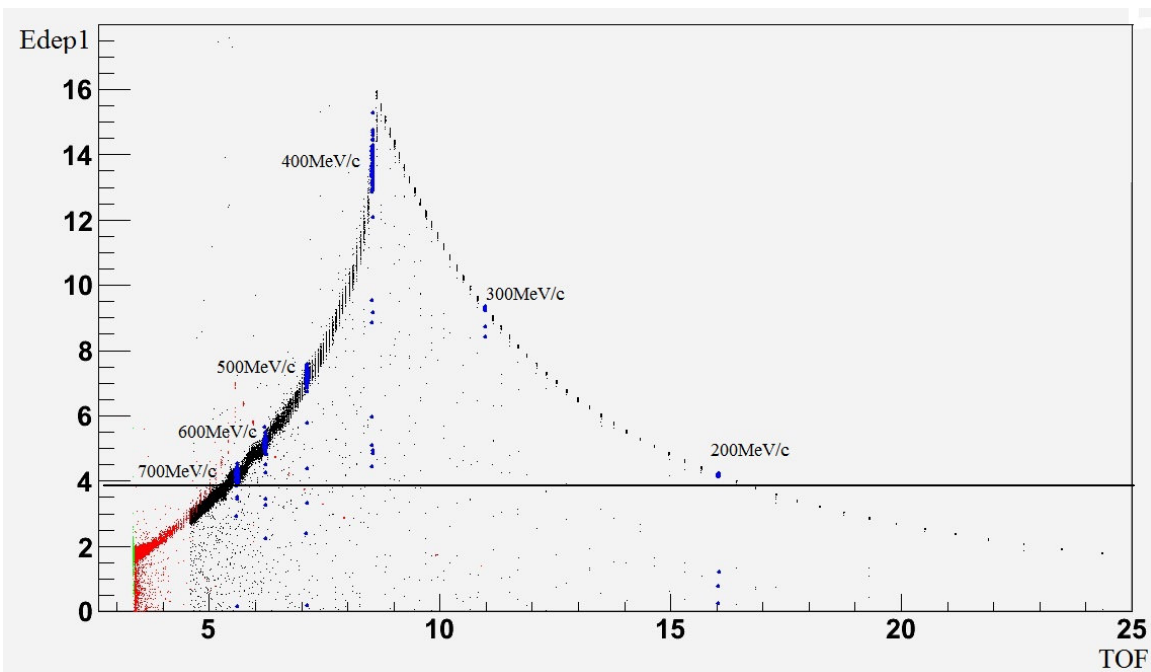

Fig I.3: Energy loss versus TOF.

To overcome the large singles rates we will set the detector threshold at 20 MeV (twice the minimum ionizing energy deposit).

I.4 Momentum resolution

The best momentum resolution is obtained by calculating the TOF per meter. From the CLAS operational experience, we know that the time resolution for the large angle counters is 200-250 ps. Figure I.4 shows the momentum calculated from the TOF compared to the momentum measured by CLAS tracking. Only protons above 80 degree in scattering angle were used.

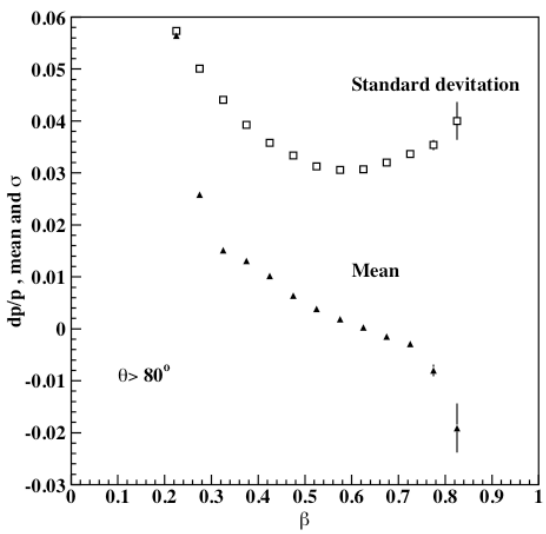

Figure I.4: The difference between the momentums determined by TOF to that determined by the tracking in CLAS. The data are for particles detected by the backward counters only.

I.5 Time resolution

Timing in the CLAS scintillators is shown in Fig. I.5. The top panel shows the distribution of measured time in the counters relative to event start time (from electrons) for large angles (>80 degree). The bottom panel shows the distribution of the same measured time, but corrected for the proton TOF, as calculated from momentum determined from energy loss in the counter. As can be seen, the time distribution gets much narrower. It is clear that random coincidences outside a window of 10 ns can be rejected.

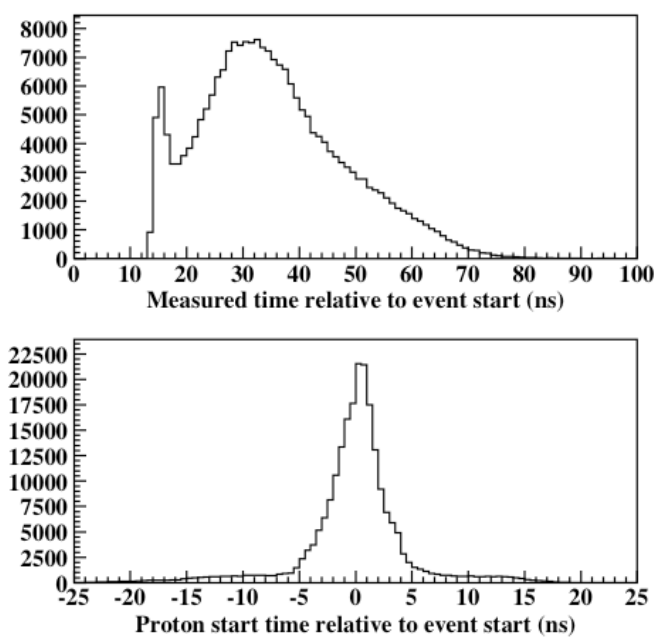

Figure I.5: The time in the backward counter relative to the electron. The top is the raw distribution and the bottom is the time after correction using the momentum as determined by the energy loss in the counter.

Appendix II: Rates: singles protons, singles electrons, signal, and background

In the following, the nucleon luminosity is assumed to be 10^{36} L cm-2 sec-1

II.1 Semi-Inclusive rates

Following [30,31] the enclosed are the differential cross sections

$$\frac{d^4\sigma}{dE_e^{'} \cdot d\Omega_e \cdot dT_2 \cdot d\Omega_2}$$

calculated for the propose kinematics, in unites of $\frac{nb}{Sr^2 \cdot GeV^2}$.

Cross sections as a function of the recoil angle [deg] and momentum [MeV/c], for x = 0.15.

$\theta_2 \setminus p_2$	***300***	***400***	***500***
90	5.577	1.163	0.754
100	5.134	1.449	0.642
110	4.706	1.274	0.534
120	4.306	1.111	0.433
130	3.947	0.965	0.343
140	3.638	0.839	0.265
150	3.389	0.737	0.202
160	3.205	0.661	0.155

Cross sections as a function of the recoil angle [deg] and momentum [MeV/c], for x = 0.37.

$\theta_2 \setminus p_2$	***300***	***400***	***500***
90	1.042	0.291	0.126
100	0.89	0.22	0.088
110	0.744	0.17	0.054
120	0.609	0.118	0.026
130	0.491	0.075	0.0088
140	0.393	0.044	1.30E-003
150	0.318	0.024	8.10E-006
160	0.265	0.013	0

The total number of semi-inclusive events for 300 Hr of beam time assuming acceptance of 50% of the backward hemisphere are given below:

Number of events as a function of the recoil angle [deg] and momentum [MeV/c], for x = 0.15

$\theta_2 \setminus p_2$	*300*	*400*	*500*	*Total*
90	**95300**	**24600**	**18600**	**138500**
100	**85100**	**29700**	**15400**	**130200**
110	**73200**	**24500**	**12000**	**109700**
120	**60600**	**19300**	**8800**	**88700**
130	**47900**	**14500**	**6000**	**68400**
140	**35800**	**10200**	**3700**	**49700**
150	**24600**	**6600**	**2100**	**33300**
160	**14300**	**3600**	**1000**	**18900**
Total	**436800**	**133000**	**67600**	**637400**

Number of events as a function of the recoil angle [deg] and momentum [MeV/c], for x = 0.37

$\theta_2 \setminus p_2$	*300*	*400*	*500*	*Total*
90	**23400**	**8100**	**4100**	**35600**
100	**19400**	**6100**	**2700**	**28200**
110	**15200**	**4300**	**1600**	**21100**
120	**11200**	**2700**	**600**	**14500**
130	**7800**	**1400**	**200**	**9400**
140	**5100**	**700**		**5800**
150	**3000**	**200**		**3200**
160	**1500**			**1500**
Total	**86600**	**23500**	**9200**	**119300**

II.2 Singles Protons

The singles proton rates are estimated based on our experience with the SRC (E01-15) experiment. In a test done before the data production and reported in [28] we found singles rates of: 3.4 10^5 for a nucleon luminosity of 3.8 10^{37} (100 μA on 0.5 mm C target) with a solid angle of 6 mSr.

For the full backward hemisphere the expected rate is:

$$singlesprotons = \frac{3.4 \cdot 10^5 \cdot (2\pi) \cdot (10^{36} L)}{3.8 \cdot 10^{37} 6msr} = 10^7 L \text{ Hz}$$

About 1/3 of these protons are above 250 MeV/c (based on our Measurement [28]) therefore:

$$Singles(above 250 Mev/c) = 3 \cdot 10^6 L$$

The singles rates on the E counters in BigBite during E01-015 were about - 80 KHz per counter at a luminosity of 5x10 ^{37} :

$$singlesprotons(250 - 600 MeV/c) = \frac{80 \cdot 10^3 60msr(10^{36} L)}{5 \cdot 10^{37} (96/24) msr} = 2.4 \cdot 10^4 L$$

For the full backward hemisphere (2π):

$$Singles(above 250 Mev/c) = 2.4 \cdot 10^6 L \text{ Hz}$$

These two measurements are consistent, and we will therefore assume a rate of

3 *10^6 L Hz of protons above 250 MeV/c* for the full backward hemisphere (2π)

The momentum distribution of the singles protons based on BigBite singles rates evaluation for the SRC experiment [28] is:

Rate = A1+A2p +A3p^2+A4p^3

A1=0.14E+4, A2=-4.18, A3=4.1E-3, A4=-0.13E-5,

where p is the momentum in MeV/c.

About 25%, 12.5%, and 8% of the singles rates above 250 MeV/c are in the 300±50, 400±50, 500±50 MeV/c bins and therefore the expected singles rate for the full backward hemisphere are:

250-350 MeV/c 8 10^5 L Hz
350-450 MeV/c 4 10^5 L Hz
450-550 MeV/c 2.5 10^5 L Hz

II.3 Singles inclusive (e,e') rates

From Ref [29] for E_{in} =10.9 GeV, E'=4 GeV and a scattered electron angle of 19^0 (E'=3 GeV / 15^0):

$$\frac{d^2\sigma}{d\Omega_{e'} \cdot dE'} = 4.5(21)\frac{nb}{SrGeV}$$

The HRS acceptances are:

$$\Delta E' = 4GeV \cdot 9\% = 0.4GeV \quad , \quad \Delta\Omega = 6mSr$$

The inclusive (e, e') rate is:

$$\frac{d^2\sigma}{d\Omega_{e'} \cdot dE'} \cdot L_d \cdot \Delta\Omega \cdot \Delta E' =$$

$$= (4.5(21) \cdot 10^{-33} cm^2 / SrGeV) \cdot (L/2 \cdot 10^{36} cm^{-2} \sec^{-1}) \cdot (6 \cdot 10^{-3} Sr) \cdot (0.4GeV) = 5(25)L$$

(L_d is the nuclear luminosity.)

II.4 Time Resolution

Neglecting the resolution in the measured time (better than 1 ns)

$$\frac{\Delta p}{p} = \frac{\Delta TOF}{TOF}$$

$$\Delta TOF = TOF \cdot \frac{\Delta P}{P} = 12meter \cdot 3.3ns \cdot \frac{1}{\beta} \cdot \frac{\Delta p}{p} = 12meter \cdot 3.3ns \cdot E / p \cdot \frac{\Delta p}{p} \approx 40 \cdot \frac{\Delta p}{p^2}$$

The momentum is given in GeV/c.

Assuming the uncertainty in the Eloss momentum resolution to be 20 MeV/c.
The largest uncertainty is for the lowest momentum:

$$\Delta TOF = 40 \cdot \frac{0.020}{0.3^2} = 8 \text{ ns.}$$

We will assume a conservative resolving time of 10 ns.

II.5 Random background rate

The rate of random coincidence events within the 10 ns resolving time for each angle/momentum bin is given by:

$$R_{(e,e')} \cdot R_{\sin gle_protonss} \cdot 10^{-8}$$

The random rates for the x'=0.6 (x'=0.25) kinematics

Momentum range	Single protons rate	Random coincidence rate
250-350	8 10^5 L Hz	0.04 (0.2)L^2 Hz
350-450	4 10^5 L Hz	0.02 (0.1)L^2 Hz
450-550	2.5 10^5 L Hz	0.013 (0.07)L^2 Hz

The number of random coincidence events in 300 hr (10 ns bin) for the different momentum/angle bins of the detected proton are given in the tables below for the two proposed kinematics:

Number of random events as a function of the recoil angle [deg] and momentum [MeV/c], for x = 0.15

$\theta_2 \setminus p_2$	***300***	***400***	***500***	***Total***
90	11950	5750	3800	21500
100	11600	5550	3700	20850
110	10900	5200	3500	19600
120	9850	4700	3150	17700
130	8500	4100	2700	15300
140	6900	3300	2200	12400
150	5100	2450	1650	9150
160	3100	1500	1000	5600
Total	67900	32550	21700	122100

Number of random events as a function of the recoil angle [deg] and momentum [MeV/c], for x = 0.37

$\theta_2 \setminus p_2$	***300***	***400***	***500***	***Total***
90	3400	1650	1100	6150
100	3300	1600	1050	5950
110	3100	1500	1000	5600
120	2800	1350	900	5050
130	2450	1150	800	4400
140	1950	950	650	3550
150	1450	700	450	2600
160	900	450	300	1650
Total	19350	9350	6250	34950

References

[1] J. J. Aubert et al. Phys. Lett. B 123,275 (1983).

[2] J. Ashman et al. Phys. Lett. B202, 603 (1988).

[3] J. Gomez et al/, Phys. Rev. D 49, 4348 (1994).

[4] M. Arneodowt et al, Phys. Lett. B211, 493 (1988).

[5] M. Arneodoet et al., Nucl. Phys. B333, 1 (1990).

[6] D. Allasia et al, Phys. Lett. B249, 366 (1990).

[7] J. Seely et al., Phys. Rev. Lett. 103, 202301 (2009).

[8] D. F. Geesaman, K. Saito and A. W. Thomas, Ann. Rev. Nucl. Part. Sci. 45, 337 (1995).

[9] P. R. Norton, Reports on Progress in Physics 66, 1253 (2003).

[10] A. De Shalit and H. Feshbach, Theoretical Nuclear Physics, Wiley, 1974.

[11] L.L. Frankfurt and M.I. Strikman, Phys. Rep. **76**, 215 (1981).

[12] L.L. Frankfurt and M.I. Strikman, Phys. Rep. **160**, 235 (1988).

[13] K.S. Egiyan et al, Phys. Rev**. C 68**, 014313 (2003).

[14] K.S. Egiyan et al, Phys. Rev. Lett. **96**, 082501 (2006).

[15] The E01-015 Experiments Website, http://hallaweb.jlab.org/experiment/E01-015.

[16] E. Piasetzky, W. Bertozzi, J. W. Watson, and S. A. Wood (spokespersons) JLab experiment E01-15 (2001).

[17] R. Shneor et al, Phys. Rev. Lett., **99**, 072501 (2007), nucl-ex/0703023.

[18] R. Subedi et al, Science 320, 1426 (2008).

[19] J. L. S. Aclander et al, Phys. Lett. **B 453**, 211 (1999).

[20] A. Malki et al. Phys. Rev. **C 65**, 015207 (2001).

[21] A. Tang et al, Phys. Rev. Lett. **90**, 042301 (2003).

[22] E. Piasetzky et al, Phys. Rev. Lett. **97**, 162504 (2006).

[23] J. Arrington, D.B. Day (spokespersons), JLab proposal E12-06-105 (2006).

[24] S. Strauch, private communication.

[25] W. Melnitchouk, M. Sargsian, and M.I.Strikman, Z. Phys. A359 (1997) 99.

[26] Ciofi degli Atti, S. Simula Phys. Lett. B319 (1993) 23.

[27] V. Palli, C. Ciofi degli Atti, L. P. Kaptari, and C. B. Mezzetti, M. Alvioli , Phys. Rev. C80, 054610 (2009).

[28] http://hallaweb.jlab.org/experiment/E01-015/documents/docs.htm:

[29] M. Sargsian CLAS –NOTE 90-007 (1970) and private communication.

[30] C. Ciofi degli Atti, L. L. Frankfurt, L. P. Kaptari, M. I. Strikman, Phys. ReV. C 76, 055206 (2007).

[31] C. Ciofi degli Atti, L. P. Kaptari, V. Palli, private communications.

[32] E. S. Smith et al., NIM 432 (1999) 265.